ISSN 1330-3651 (Print), ISSN 1848-6339 (Online) https://doi.org/10.17559/TV-20220622043203
Preliminary communication

# Prediction of Depth Distribution Curve of Dissolution Rates Based on the Undulating Features of Rock Surfaces

Xianfa CAO, Yingding HE, Zhantuo SONG*, Hailing LI, Gangchen SUN, Jingyan LAN

**Abstract:** In karst regions, the drilling into the rock layer is restricted, if the construction site has a thick overburden and a small upper load. The evaluation of karst development features beneath the site becomes a common technical difficulty in building foundation engineering. Drawing on our previous research into the depth distribution features of dissolution rate, this paper collects 1000 plus data on typical karst regions across China, and selects 65 data for detailed analysis. Specifically, the rock surface dissolution features were analyzed on the top and bottom of the strong dissolution zone, and used to set up the control conditions for the top and bottom predictions of the strong dissolution zone. On this basis, the authors provided a prediction method for the depth distribution curve of dissolution rates. The results show that the elevation of 75% dissolution rate can be regarded as the top elevation of the strong dissolution zone at the site, which controls the prediction error within 0.5 m. If the pores and fissures are not so developed at the karst site, the elevation of 15% dissolution rate can be regarded as the bottom elevation of the strong dissolution zone at the site. According to the top and bottom elevations, the authors derived the predicted curve of the depth distribution function for the dissolution rates at each site. The predicted curve basically overlapped the curve and scatterplot of the dissolution rates measured at the site, a sign of reliable prediction. The proposed prediction method for the depth distribution curve of the dissolution rates at karst construction sites mainly applies to the sites with undeveloped to moderately developed pores and fissures. Further research is needed to verify its effectiveness in sites with strongly developed pores and fissures.

**Keywords:** karst; karst development; rock surface undulation; strong dissolution zone

## 1 INTRODUCTION

In karst regions, one of the basic tasks of engineering survey is to clarify the karst features at the construction site. If a construction project takes place in karst regions, the drilling into the rock layer is restricted, if the construction site has a thick overburden and a small upper load. The boreholes can only reach the bedrock layer. In the event that the overburden thickness of the karst site exceeds 5 meters, usually the composite foundation or natural foundation is directly employed for buildings or plants below 6 floors, and the geological prospecting generally does not penetrate into the rock. Engineering projects of this kind are rather common in Southwest China. And in fact, such projects account for some 5 - 12% of the engineering prospecting projects in karst areas, according to the statistics of several class A prospecting institutions in karst areas in Guangxi in recent three to five years.

Formation lithology, groundwater and geological structure constitute the main factors that affect the karst development features of the site [1, 2]. And therefore, such influencing factors can serve for regional and large-scale karst features analysis and as assessment indicators [3, 4]. At the time being, the assessment theory mostly relies on karst caves' development, which will be exposed after rock drilling, yet the rock surface fluctuation features have not merited enough attention. Then, it is important to predict the karst features at the site according to the undulating features of the bedrock layer. In fact, this has long been a practical difficulty in karst engineering.

At present, due to the high drilling and prospecting cost, and the impossibility of acquiring continuous geological profile between the two boreholes, karst geophysical prospecting is the primary means to study the karst features underground. In karst engineering, geological radar [5-9], cross-hole computed tomography (CT) [10-12], and high-density electronic method [13, 14] have been widely tested, while micro-gravity [15, 16] and tube-wave method [17] have been developed. In engineering practice, multiple geophysical prospecting methods are usually applied synthetically, rather than used independently [18-22]. However, there are a wealth of factors affecting the detection accuracy and applicability of geophysical prospecting technology, among which groundwater is the most common one that influences the application of geophysical exploration in karst areas in China. There is medium or abundant groundwater under the most of construction sites in karst areas of southwest China, which directly undermines the detection depth and accuracy of karst physical prospecting technology in such sites; as a result, the technology's applicability faces severe challenges of being widely applied by engineering institutions. Given this situation, drilling method still dominates the karst prospecting in engineering practice, whereas the geophysical detection method has not been widely used.

In the current engineering practice, drilling remains the most applicable, popular, and reliable method for evaluating the karst features at the site. In our previous research [23-24], the authors theorized the law that the dissolution degree of karst foundations attenuates exponentially with the growing depth, established a quantitative analysis method for the depth distribution function of dissolution rate, presented the determination method and standard for top and bottom elevations of the strong dissolution zone, and developed an evaluation model for the karst degree based on the features of the strong dissolution zone. This research solved the long-standing difficulties of quantitatively measuring the depth variation law of building foundation dissolution degree in karst areas; and in terms of categorizing the strong dissolution zone, this research has incorporated the two dissolution types of rock face dissolution and cavernous dissolution, and made them as the assessment index of karst development degree. With such endeavor, the influence of rock surface's dissolution features can be fully manifested, which shed a light on the karst features assessment of building foundation [25]. Nevertheless, the above theoretical results only apply to project sites with

dense boreholes and deep drilling depth. With respect to the site without rock prospecting, or the prospecting depth merely reaches the rock surface, nevertheless, the issue of predicting the depth distribution curve of the site's dissolution rate is based on the limited information of rock surface undulation, and then providing references for determining the boundary of strong dissolution zone, still requires further study at length.

Drawing on our previous research, this paper analyzes the statistical features of the rock surface dissolution rates at the top and bottom of the strong dissolution zone, and presents the prediction methods for the top and bottom elevations of the zone. Based on the predicted top and bottom elevations, the authors established a prediction method for the depth distribution curve of the strong dissolution zone at the site, combined with the depth distribution function of the zone. The reasonability of the predicted results was demonstrated.

## 2 CONTROL CONDITIONS

Southwest China boasts some of the most typical karst regions in the world. In our previous research, 1,000-plus data on construction projects were collected from the karst regions in Southwest China. In this study, 65 data were selected randomly, including 4 in Shenzhen City, Guangdong Province, 4 in Longyan City, Fujian Province, 4 in Kunming City, Yunnan Province, 4 in Guizhou Province, and 4 in Chongqing Municipalities. The other data were from contiguous karst regions in Nanjing, Liuzhou, Guilin, Chongzuo, Laibin, and Hechi, Guangxi Zhuang Autonomous Region. The selected karst project sites, belonging to the elevation range of 5 m - 2100 m, cover various landforms (from low mountains and hills to high mountains and basins), and span across tropical climate and subtropical climate. These sites differ significantly in engineering geology and hydrogeology. They can basically represent the karst geology in most carbonate rock sites.

At each site, the dissolution rates of rock surface at the top and bottom of the strong dissolution zone can be solved in the following steps: Firstly, the depth distribution curve of the rock surface dissolution rates at the site is calculated by Cao et al. [26]. Next, the criteria for determining the tops and bottoms of the zone provided by Cao et al. for the top and bottom of that zone [21] are: The top of the zone has a dissolution rate of 75%, and the bottom has a dissolution rate of 25%. According to these criteria, the top and bottom elevations of the strong dissolution can be determined. Finally, the rock surface dissolution rates corresponding to the top and bottom elevations are determined. The specific method is as follows: as in Fig. 1, the total dissolution rate curve $F(H)$ and the rock face dissolution rate curve $S(H)$ were plotted in the same coordinate system $H$-$R$ ($H$ stands for the elevation, $R$ represents the total dissolution rate or rock surface dissolution rate). Then this research drew up two straight lines on the coordinate axis with the total corrosion rate $P$ of 75% and 25% respectively, and therefore, the two straight lines intersected the total dissolution rate curve $F(H)$, and $f_1$ and $f_2$ were two intersections. The elevation corresponding to these two intersections represented the upper boundary elevation and lower boundary elevation of the strong dissolution. Then these two intersections were projected to the elevation $H$ axis, and their projection lines intersected surface erosion rate curve $S(H)$ with the $s_1$ and $s_2$ as the intersections. The projection coordinates $r_1$ and $r_2$ of the points $s_1$ and $s_2$ on the $R$-axis, in fact, represented the requested surface erosion rate corresponding to the upper and lower boundaries of the strong dissolution zone, respectively.

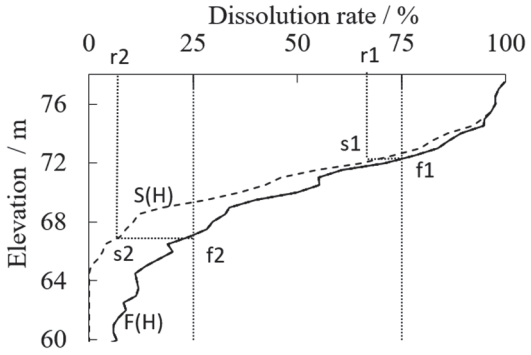


**Figure 1** The curve relationship between the boundary elevation of the strong dissolution zone and the dissolution rate of the rock surface

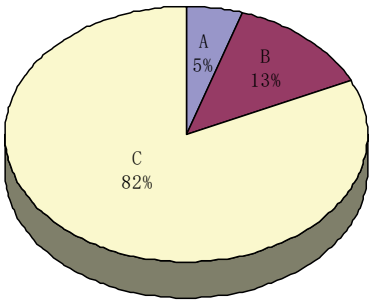


**Figure 2** Statistical distribution of top rock surface dissolution rate of strong dissolution zone

Following the above method, the rock surface dissolution rates of the strong dissolution zone at each site are summarized in Fig. 2 and Fig. 3. In Fig. 2, A, B, and C represent the percentage of the sites with the rock surface dissolution rate at the top elevation being smaller than 60%, between 60% and 70%, and greater than 70%, respectively. In Fig. 3, A, B, C, D, and E represent the percentage of the sites with the rock surface dissolution rate at the bottom elevation falling in 0 - 5%, 5 - 10%, 10 - 15%, 15 - 20%, and 20 - 25%, respectively.

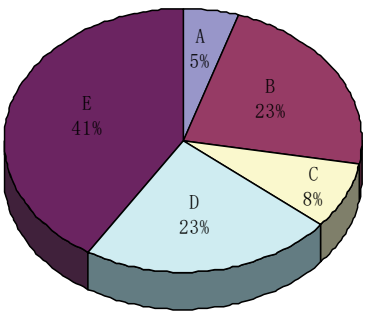


**Figure 3** Statistical distribution of bottom rock surface dissolution rate of strong dissolution zone

As shown in Fig. 2, more than 80% of the sites have a top rock surface dissolution rate greater than 70%. Only 65% of all sites have a rate smaller than 65%. Besides, the

top rock surface dissolution rate of strong dissolution zone at the sites minimizes at 58.4%, and maximizes at 75%, with a mean of 72.7%, and a standard deviation of 3.814%. The top elevation dissolution is mainly composed of rock surface dissolution. The dissolution of pores and fissures accounts for a very small portion of top elevation dissolution. The top elevation of the strong dissolution zone is the dividing line between the soil layer and the strong dissolution zone. The greater the top dissolution rate, the more uniform the foundation, and the safer the project design. Thus, the standard value $r_{sc}^{'}$ of the rock surface dissolution rate at the top elevation of the strong dissolution zone can be calculated by:

$$r_{sc}^{'} = \left[1 + \left(\frac{1.704}{\sqrt{n}} + \frac{4.678}{n^2}\right) \cdot \delta\right] \cdot \bar{r}_{sc}^{'} \tag{1}$$

where, $\bar{r}_{sc}^{'}$ is the mean rock surface dissolution rate at the top elevation of the strong dissolution zone; $\delta$ is the coefficient of variation; $n$ is the number of statistical samples.

In this case, the parameter n is 65, $r_{sc}^{'}$ is 72.7%, $\delta$ is 0.0525. Thus, it can be obtained that the standard value of our samples is 73.6%, with a very small difference (1.4%) from the critical dissolution rate at the top elevation of the strong dissolution zone. Therefore, the top elevation of the zone mainly depends on the degree of rock surface dissolution at the site. When no rock drilling takes place, the rock surface dissolution rate of 75% can serve as the control condition for predicting the top elevation of the strong dissolution zone.

As shown in Fig. 3, 41% of the sites have a bottom rock surface dissolution rate of 20% - 25%. Quite many sites belong to the other intervals of bottom rock surface dissolution rate. According to the rock surface dissolution rate at the bottom boundary of the strong dissolution zone, the statistical standard deviation is 0.098 and the variation coefficient is as high as 0.465. This means the sites differ significantly in the proportions of rock surface dissolution rate and pores / fissures dissolution rate at the bottom of the strong dissolution zone. The bottom elevation cannot be simply predicted based on either rate. To a certain extent, the result suggests the direction of karst development: dissolution generally occurs on the rock surface first, and gradually extends to the interior of the rock mass. The proportion difference among the sites is precisely the result of the fact that pores and fissures develop later than rock surface dissolution. As a result, the prediction of karst development at the site based on the undulating features of the rock surface mainly applies to the sites with no or moderately developed pores and fissures. If the site has strong/extremely strong development of pores and fissures, the prediction result of this approach can only serve as a reference. According to the collected data and Cao et al. work [19], the pores/fissures development at the site is closely correlated with rock surface undulation. The greater the undulation, the more intense the development. Thus, the reliability of the prediction result can be judged by the undulation features of the rock surface at the site.

It can be seen from Fig. 3 that the bottom rock surface dissolution rate minimizes at 0, and maximizes at 25%, with a mean of 16.2%, and the coefficient of variation $\delta$ *of* 0.465. The standard value $r_{sc}$ of the rock surface dissolution rate at the bottom elevation of the strong dissolution zone can be calculated by:

$$r_{sc} = \left[1 - \left(\frac{1.704}{\sqrt{n}} + \frac{4.678}{n^2}\right) \cdot \delta\right] \cdot \bar{r}_{sc} \tag{2}$$

where, $\bar{r}_{sc}$ is the mean rock surface dissolution rate at the bottom elevation of the strong dissolution zone; $n$ is the number of statistical samples.

Thus, it can be obtained that the standard value of our samples is 14.6%, with a difference of 10.5% from the bottom dissolution rate. This implies that pores/fissures development and rock surface dissolution both greatly affect the bottom elevation of the strong dissolution zone. Hence, the rock surface dissolution rate of 15% can serve as the control condition for predicting the bottom elevation of the strong dissolution zone.

## 3 CURVE PREDICTION

The above analysis shows that, when the depth distribution curve of the rock surface dissolution rate at the site is known, the predicted top elevation of the strong dissolution zone is the elevation corresponding to the top rock surface dissolution rate of 75% on the rock surface dissolution curve, while the predicted bottom elevation of the strong dissolution zone is the elevation corresponding to the bottom rock surface dissolution rate of 15% on the rock surface dissolution curve. The two points on the curve are denoted as $P_1$ = (75%, $H_{cr}^{'}$) and $P_2$ = (25%, $H_{cr}$), respectively ($H_{cr}^{'}$ is top elevation of the strong dissolution zone and $H_{cr}$ is bottom elevation of the strong dissolution zone [25]).

The depth distribution function of dissolution rates can be expressed as:

$$r = ae^{b(H-H_0)} \tag{3}$$

where, $a$ and $b$ are constant; $H_0$ is the elevation of the start point.

Substituting two predicted points $P_1$ and $P_2$ into Eq. (3), the following set of equations can be obtained:

$$\begin{cases} 0.75 = ae^{b\left(H_{cr}^{'} - H_0\right)} \\ 0.25 = ae^{b\left(H_{cr} - H_0\right)} \end{cases} \tag{4}$$

Solving the set of Eq. (4), the two coefficients a and b of the depth distribution function at the site can be obtained. On this basis, it is possible to predict the depth distribution curve of dissolution rates.

Under the control condition of the rock surface dissolution rate of 15%, the predicted bottom elevation of the strong dissolution zone is denoted as $H_R$. For any site whose bottom rock surface dissolution rate is greater than

15%, the bottom elevation $H_{CR}$ of its strong dissolution zone must surpass $H_R$. That is, the prospecting depth has reached $H_R$, and penetrated the bottom of the strong dissolution zone at the site. In this case, the predicted result is safe in engineering. For any site whose bottom rock surface dissolution rate is smaller than 15%, the bottom elevation $H_{CR}$ of its strong dissolution zone must fall short of $H_R$. That is, the prospecting depth has not reached the bottom of the zone. In this case, the predicted result is unsafe in engineering. Therefore, this paper selects the 10 sites, whose bottom rock surface dissolution rate is smaller than 15%, from the 65 samples, and analyzes the reasonability of their predicted results. The overview of the sites and predicted top and bottom elevations of the strong dissolution zone are displayed in Tab. 1.

**Table 1** Overview of the sites and predicted top and bottom elevations of the strong dissolution zone

| Site name | Code | Total number of boreholes | Borehole encountering rate / % | Linear karst rate / % | Top elevation of strong dissolution zone / m | | | Bottom elevation of strong dissolution zone /m | | |
|---|---|---|---|---|---|---|---|---|---|---|
| | | | | | Actual value | Predicted value | Error | Actual value | Predicted value | Error |
| Budlings 17 - 19, Fucheng International, Rong'an County, Liuzhou City, Guangxi Zhuang Autonomous Region, China | Site 1 | 24 | 25.0 | 11.2 | 113.2 | 113.3 | 0.1 | 109.8 | 109.6 | 0.2 |
| West Area, Guilin Library, Guangxi Zhuang Autonomous Region, China | Site 2 | 72 | 16.7 | 3.6 | 154.3 | 154.3 | 0 | 152.2 | 152.3 | 0.1 |
| Building 5, Jinsheng Plaza, Liuzhou City, Guangxi Zhuang Autonomous Region, China | Site 3 | 85 | 55.3 | 17.3 | 72.4 | 72.4 | 0 | 66.8 | 66.3 | 0.5 |
| Building 2, JiachengNana'an, Laibin City, Guangxi Zhuang Autonomous Region, China | Site 4 | 76 | 51.3 | 16.9 | 69.9 | 70.3 | 0.4 | 62.8 | 60.8 | 2.0 |
| Building 3, JiachengNana'an, Laibin City, Guangxi Zhuang Autonomous Region, China | Site 5 | 59 | 45.8 | 21.3 | 72.3 | 72.8 | 0.5 | 64.9 | 64.7 | 0.2 |
| Building 4, Zazuo Old City Reconstruction Site, Xiuwen County, Guiyang City, Guizhou Province, China | Site 6 | 51 | 27.5 | 8.02 | 1285.3 | 1285.3 | 0 | 1281.3 | 1280.9 | 0.4 |
| Building 5, Qianlong Sunny Yuyuan, Xiushan County, Chongqing Municipality, China | Site 7 | 29 | 72.4 | 20.4 | 338.8 | 339.1 | 0.3 | 332.2 | 334.4 | 2.2 |
| Central South Area, Block A2, Public Rental Housing, Airport Economic Zone, Kunming City, Yunnan Province, China | Site 8 | 17 | 76.5 | 10.0 | 2084.1 | 2084.7 | 0.6 | 2073.8 | 2073 | 0.8 |
| East Zone, Crown International, Longyan City, Fujian Province, China | Site 9 | 49 | 46 | 18.3 | 287.5 | 287.7 | 0.2 | 274.2 | 275.3 | 1.1 |
| East Area, Refrigeration Workshop, Fengrunfeng Investment Co., Ltd., Shenzhen City, Guangdong Province, China | Site 10 | 131 | 46.6 | 20.0 | 26.1 | 26.2 | 0.1 | 20.3 | 19.9 | 0.4 |

As shown in Tab. 1, the error between the predicted and actual top elevations of the strong dissolution zone maximized at 0.6 m, and minimized at 0 m. The error was smaller than 0.5 m at most sites. As for the 55 sites not included in Tab. 1, the predicted value was all zero. Overall, the prediction error of the top elevation of the strong dissolution zone is smaller than 0.5 m in more than 98% of the sites, and smaller than 0.3 m in more than 95% of the sites. Therefore, our prediction model can predict the top elevation of the strong dissolution zone at the sites very reliably.

Meanwhile, the error between the predicted and actual bottom elevations of the strong dissolution zone maximized at 2.2 m, and minimized at 0.1 m. The error surpassed 2.0 m at two sites (Site 4 and Site 7), fell between 1.0 m and 2.0 m at one site (Site 9), ranged between 0.5 m and 1.0 m at two sites (Site 3 and Site 8), and stayed below 0.5 m at the remaining five sites. As for the 55 sites not included in Tab. 1, the prediction error of the bottom elevation was smaller than 0.3. Overall, the prediction error of the bottom elevation of the strong dissolution zone is smaller than 0.5 m in more than 92% of the sites. Hence, the prediction accuracy can meet the accuracy requirements of most projects, if the rock surface dissolution rate of 15% is adopted as the control condition for predicting the bottom elevation of the strong dissolution zone.

The sites listed in Tab. 1 have the greatest prediction error of the bottom elevation of the strong dissolution zone among all research samples. As far as these sites are concerned, the borehole encountering rate minimized at 25%, and maximized at 76.5%; the linear karst rate minimized at 7.4%, and maximized at 30.9%. Here, the strong karst development is defined as the borehole encountering rate $\geq$ 30%, or the linear karst rate $\geq$ 20%; the moderate karst development is defined as the borehole encountering rate of (10%, 30%), or the linear karst rate of (5%, 20%). By these definitions, only three sites (Sites 1, 2, and 6) among those in Tab. 1 witness moderate karst development. At these sites, the prediction error of the top elevation of the strong dissolution zone maximized at 0.1 m, and that of the bottom elevation of the strong dissolution zone maximized at 0.4 m. The prediction errors were much smaller than those of the other 7 sites with strong karst development. Hence, borehole encountering rate and linear karst rate essentially measure the pores/fissure development at each site. The precision and reliability of our prediction method mainly hinge on the degree of pores/fissure development.

According to the predicted top and bottom elevations of the strong dissolution zone, the depth distribution curve of the dissolution rate at each site can be obtained by the method introduced in the preceding section (Fig. 4).

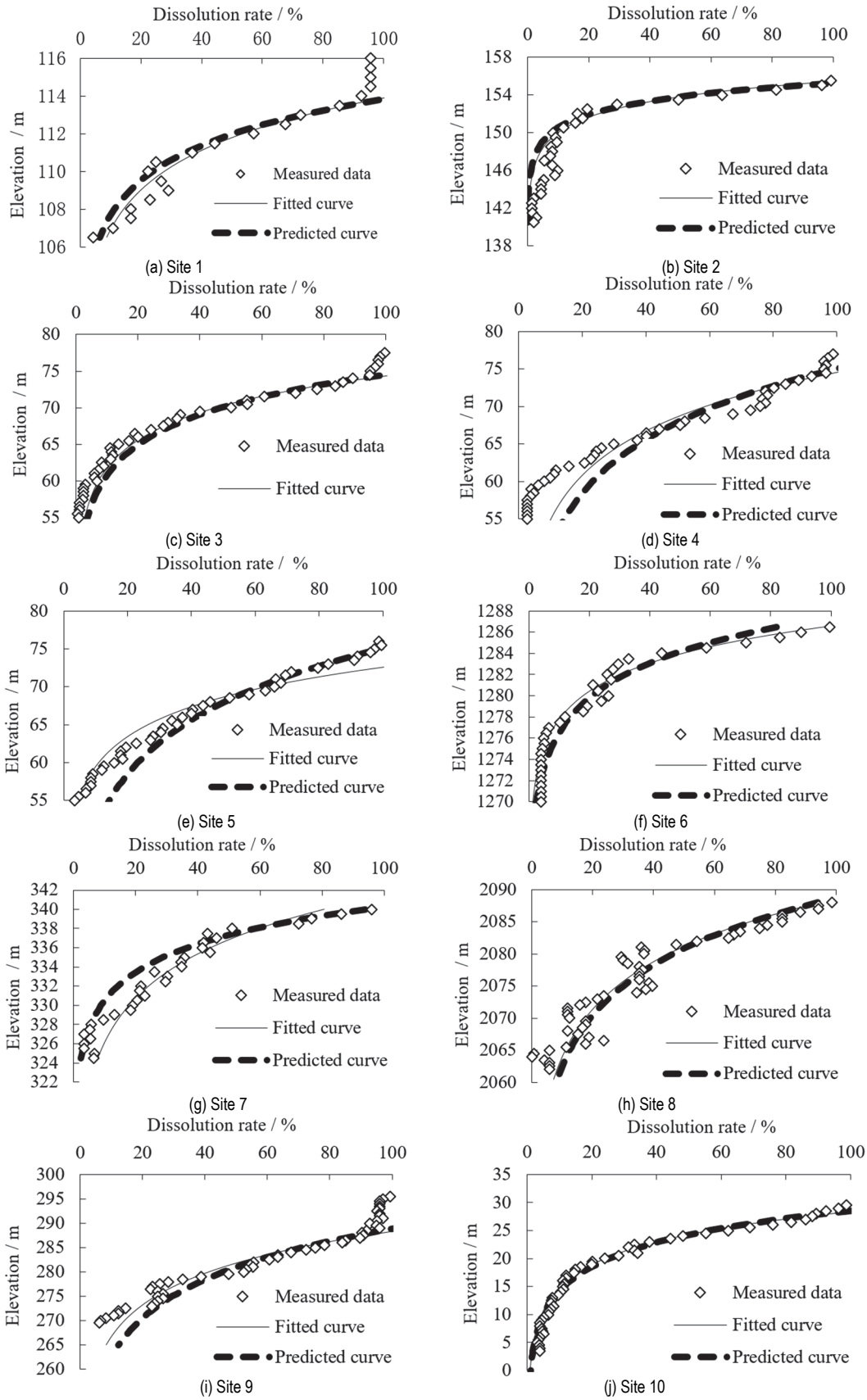


**Figure 4** Depth distribution of predicted dissolution rates at different sites

As shown in Fig. 4, the curve fitted from the scatterplot of the measure dissolution rates at each site, and the predicted curve both oscillated near the measured curve by similar amplitudes. For Sites 2, 3, 6, 8, and 10, the predicted curve basically overlapped the measured data. For Sites 4 and 7, the predicted curve above the top

elevation of the strong dissolution zone basically overlapped the measured data, and that below the top elevation was consistent with the distribution area in the measured scatterplot. Hence, the predicted curves of these sites are reasonable. As for Site 5, the upper part of the predicted curve overlapped the measured scatterplot, and the lower part and the fitted curve contained the measured scatterplot. Therefore, the predicted curve of this site is also reasonable. The proposed prediction method for depth distribution of dissolution rate at construction sites is rational, although the prediction accuracy of the top elevation of strong dissolution zone may be affected by the development of pores and fissures.

Our method made reasonable predictions on all the sample sites with strong development of pores and fissures. Given the diversity and complexity of karst engineering sites, and the limited sample size, the authors recommended to apply the prediction model mainly to the sites with no to moderate development of pores and fissures, and treat the prediction results are a reference for the sites with strong pores / fissures development.

## 4 CONCLUSIONS

(1) The top elevation dissolution is mainly composed of rock surface dissolution. The dissolution of pores and fissures accounts for a very small portion of top elevation dissolution. Therefore, the elevation corresponding to the rock surface dissolution rate of 75% can serve as the predicted top elevation of the strong dissolution zone at the site. Under this control condition, the prediction error can be generally controlled within 0.5 m, which fully meets the precision required for engineering practice.

(2) Pores/fissures dissolution and rock surface dissolution are the main types of dissolution at the bottom elevation of the strong dissolution zone. For the karst sites with non-intense pores/fissures development, the elevation corresponding to the rock surface dissolution rate of 15% can serve as the predicted bottom elevation of the strong dissolution zone at the site. Under this control condition, the prediction error falls within the allowed range of engineering.

(3) The top and bottom elevations of the strong dissolution zone, which are predicted from the depth distribution curve of rock surface dissolution rates, can be used to predict the depth distribution of dissolution rates at the site. The predicted curves basically overlapped the curves and scatterplots of measured dissolution rates, indicating the reliability of the prediction model.

(4) The proposed prediction method for the depth distribution curve of the dissolution rates at karst construction sites mainly applies to the sites with undeveloped to moderately developed pores and fissures. Further research is needed to verify its effectiveness in sites with strongly developed pores and fissures.

### Acknowledgements

The financial supports from the Guangxi Natural Science Foundation of China (Grant No.: 2020GXNSFAA297078); The National Natural Science Foundation of China (Grant No.: 52168067, Grant No.: 41867039) are greatly acknowledged.

## 5 REFERENCES

[1] Veress, M. (2020). Karst types and their karstification. *Journal of Earth Science*, *31*(3), 621-634. https://doi.org/10.1007/s12583-020-1306-x

[2] Lu, Y., Liu, Q., & Zhang, F. E. (2013). Environmental characteristics of karst in China and their effect on engineering. *Carbonates and Evaporites*, *28*(1), 251-258. https://doi.org/10.1007/s13146-013-0158-1

[3] Duan, Y., Xie, Z., Zhao, F., Zeng, H., Lin, M., Chen, H., & Hou, Z. (2021). Suitability of Underground Space Development in Plateau Cities Basedon Geological Environment Analysis: Case Studyin Kunming, China. *Journal of Urban Planning and Development*, *147*(2), 05021014.

[4] Wang, Y., Jing, H., Yu, L., Su, H., & Luo, N. (2017). Set pair analysis for risk assessment of water inrush in karst tunnels. *Bulletin of Engineering Geologyand the Environment*, *76*(3), 1199-1207. https://doi.org/10.1007/s10064-016-0918-y

[5] Putiška, R., Marschalko, M., Yilmaz, I., Niemiec, D., Cheng, X., Dostal, I., & Kubáč, J. (2021). Surface Geophysical Methodsused to Verify the Karst Geological Structurein the Built-up Area: A Case Study of Specific Engineering-Geological Conditions. *Acta Geologica Sinica-English Edition*, *95*(5), 1763-1770. https://doi.org/10.1111/1755-6724.14761

[6] Su, M., Zhao, Y., Xue, Y., Wang, P., Xia, T., Zhang, K., & Li, C. (2021). Progressive fine integrated geophysical method for karst detection during subway construction. *Pureand Applied Geophysics*, *178*(1), 91-106. https://doi.org/10.1007/s00024-020-02636-4

[7] Wang, J., Li, L., Shi, S., Sun, S., Ba, X., & Zhang, Y. (2019). Fine exploration and control of subway crossing karstarea. *Applied Sciences*, *9*(13), 2588. https://doi.org/10.3390/app9132588

[8] Xie, P., Wen, H., Xiao, P., Zhang, Y. (2018). Evaluation of ground-penetrating radar (GPR) and geology survey for slope stability study in mantled karst region. *Environmental earths ciences*, *77*(4), 1-12. https://doi.org/10.1007/s12665-018-7306-9

[9] Caselle, C., Bonetto, S., Comina, C., & Stocco, S. (2020). GPR surveys for the prevention of karst risk in underground gypsum quarries. *Tunnelling and Underground Space Technology*, *95*, 103137. https://doi.org/10.1016/j.tust.2019.103137

[10] Peng, D., Cheng, F., Liu, J., Zong, Y., Yu, M., Hu, G., & Xiong, X. (2021). Joint to mography of multi-cross-holeand bore hole-to-surface seismic data for karst detection. *Journal of Applied Geophysics*, *184*, 104252. https://doi.org/10.1016/j.jappgeo.2020.104252

[11] Su, M., Liu, Y., Xue, Y., Qu, C., Wang, P., & Zhao, Y. (2020). Detection method of pile foundation on subway lines based on cross-hole resistivity computed tomography. *Journalof Performance of Constructed Facilities*, *34*(6), 04020103.

[12] Zhang, H., Zhang, G., & Wang, Y. (2020). Experimental study on the detection of karst pores and water-bearing state by cross-hole CT imaging in karst faulted basin. *Carsologica Sinica*, *39*(5), 737-744. https://doi.org/10.1021/acsaem.0c02600

[13] Jianjun, G., Zhang, Y. X., & Xiao, L. (2020). An application of the high-density electrical resistivity method for detecting slide zones in deep-seated landslides in limestone areas. *Journal of Applied Geophysics*, *177*, 104013. https://doi.org/10.1016/j.jappgeo.2020.104013

[14] Jingjing, C. A. I., Changhong, Y. A. N., Ning, W. A. N. G., Yong, S. H. A. O., Jun, Z. H. E. N. G., & Zhigang, T. A. N. G. (2011). Application of high-density resistivity method to

karst investigation of metro engineering. *Journal of Engineering Geology*, *19*(6), 935-940.

[15] Solbakk, T., Fichler, C., Wheeler, W. H., Lauritzen, S. E., & Ringrose, P. (2018). Detecting multi scale karst features including hidden cave susing micro gravimetry in a Caledoniann appesetting: Mefjell massif, Norway. *Norwegian journal of geology*, *98*(3), 359-378. https://doi.org/10.17850/njg98-3-04

[16] Pazzi, V., Di Filippo, M., Di Nezza, M., Carlà, T., Bardi, F., Marini, F., & Fanti, R. (2018). Integrated geophysical survey in a sinkhole-prone area: Microgravity,electrical resistivity to mographies, and seismic noise measurements to delimit its extension. *Engineering Geology*, *243*, 282-293. https://doi.org/10.1016/j.enggeo.2018.07.016

[17] Yang, J., Li, X. W., & Sun, X. L. (2020). Extension of tube wave detection for quality evaluation of pile foundation. *Geophysical Prospecting*, *68*(5), 1476-1491. https://doi.org/10.1111/1365-2478.12934

[18] Gołębiowski, T. & Jarosińska, E. (2019). Application of GPR and ERT methods for recognizing of gypsum deposits in urban areas. *Acta Geophysica*, *67*(6), 2015-2030. https://doi.org/10.1007/s11600-019-00370-7

[19] Shaaban, F., Ismail, A., Massoud, U., Mesbah, H., Lethy, A., & Abbas, A. M. (2013). Geotechnical assessment of ground conditions around a tilted building in Cairo-Egypt using geophysical approaches. *Journal of the Association of Arab Universities for Basic and Applied Sciences*, *13*(1), 63-72. https://doi.org/10.1016/j.jaubas.2012.06.002

[20] Cueto, M., Olona, J., Fernández-Viejo, G., Pando, L., & López-Fernández, C. (2018). Karst-induced sinkhole detection using an integrated geophysical survey: a case study along the Riyadh Metro Line 3(Saudi Arabia). *Near Surface Geophysics*, *16*(3), 270-281. https://doi.org/10.3997/1873-0604.2018003

[21] Shangxin, F., Yufei, Z., Yujie, W., Shanyong, W., & Ruilang, C. (2020). A comprehensive approach to karst identification and groutability evaluation-A case study of the Dehou reservoir, SW China. *Engineering Geology*, *269*, 105529. https://doi.org/10.1016/j.enggeo.2020.105529

[22] Zhang, K., Tannant, D. D., Zheng, W., Chen, S., & Tan, X. (2018). Prediction of karst for tunneling using fuzzy assessment combined with geological investigations. *Tunnelling and Underground Space Technology*, *80*, 64-77. https://doi.org/10.1016/j.tust.2018.06.009

[23] Cao, X. F., Zhang, J. S., & Liu, Z. K. (2014). Dissolution degree and depth distribution of karst building foundation. *Journal of Central South University (Scienceand Technology)*, *45*(8), 2787-2792.

[24] Cao, X. F., Zhang, J. S., & Liu, Z. K. (2014). Quantitative analys is method of dissolution degree distribution characteristics with elevation. *Journal of Central South University (Scienceand Technology)*, *45*(7), 2339-2345.

[25] Cao, X. F., Liu, Z. K., & Li, H. L. (2015). Division of strongd is solution zone in karst building foundation. *Hydrogeology and Engineering Geology*, *42*(6), 91-95.

[26] Zhang, B. H., Xie, Y. H., Li, H. L., & Liu, B. C. (2020). Distribution Pattern of Rock Face Dissolution Degree with Depth in Building Foundationin the Karst Terrain of South west China. *International Journal of Design and Nature and Ecodynamics*, *15*(2), 261-268. https://doi.org/10.18280/ijdne.150217

**Contact information:**

**Xianfa CAO**
College of Civil and Architectural Engineering,
Guilin University of Technology,
Guilin 541004, China
E-mail: caoxianfa@126.com

**Yingding HE**
College of Civil and Architectural Engineering,
Guilin University of Technology,
Guilin 541004, China
E-mail: heyingding@126.com

**Zhantu SONG**
(Corresponding author)
Guangxi Huanan Geotechnical Engineering Co. Ltd,
Nanning 530001, China
E-mail: gxjcszht@126.com

**Hailing LI**
College of Civil and Architectural Engineering,
Guilin University of Technology,
Guilin 541004, China
E-mail: lhl0102@126.com

**Gangchen SUN**
College of Civil and Architectural Engineering,
Guilin University of Technology,
Guilin 541004, China
E-mail: sun2963@163.com

**Jingyan LAN**
College of Civil and Architectural Engineering,
Guilin University of Technology,
Guilin 541004, China
E-mail: lanjy1999@163.com